MecSol2013
International Symposium on Solid Mechanics
April 18-19, 2013
Porto Alegre, Rio Grande do Sul, Brazil

A Geometrically Nonlinear Simplified Beam Element with Linear Viscoelastic Behaviour

Simone ClaudianoSemptikovski
Department of Mechanical Engineering
Universidade do Estado de Santa Catarina
simone.sempt@gmail.com

Pablo A. Muñoz-Rojas
Department of Mechanical Engineering
Universidade do Estado de Santa Catarina
pablo@joinville.udesc.br

ABSTRACT

In recent years, the use of pipes made of high density polyethylene (HDPE) has registered a remarkable increase in submersed applications for gas and water distribution. Often, the submersion process is a challenging engineering problem due to the high curvature to which the pipes are submitted, and to the requirement of a nonlinear dynamic analysis. Computational systems, which adopt truss and beam models, have been employed to predict the pipelines mechanical behaviour. The latter are more accurate than the former but demand more memory storage and a high computational effort. In this work, as a first step towards modeling HDPE submersed pipes, a linear viscoelastic geometrically nonlinear beam finite element is formulated by modifying a geometrically nonlinear truss element. Bending stiffness is introduced by means of rotational springs between two adjacent bar elements, keeping only translational degrees of freedom. This results in an element with 6 degrees of freedom per element, compared to 12 degrees of freedom per element for the traditional Euler-Bernoulli and Timoshenko beam formulations. The internal force vector and the stiffness matrix are derived using the principle of virtual work. Special care is taken to develop the exact tangent stiffness matrix so that quadratic convergence rate can be expected in the Newton-Raphson solution process. Linear viscoelastic behaviour is modeled using Kelvin-Voigt and Maxwell rheological models and a numerical algorithm to perform the interconversion of the material parameters between them is applied. Creep compliance and relaxation functions are modeled using Prony series. The discretization in time is performed using both implicit and explicit approaches. Results are compared to the finite element commercial software MSC Marc, whose Euler-Bernoulli beam element uses cubic interpolation functions (Hermite) and has 12 degrees of freedom per element. In addition to the excellent agreement of results verified, the proposed element yields a much smaller system of equations and has potential for great numerical efficiency.

Keywords: Simplified Bending Stiffness. Geometric Nonlinearity.Linear Viscoelasticity.

1 INTRODUCTION

Submerged pipelines of high density polyethylene (HDPE) have been used for water and sewage transportation since 1960 [1] and more recently for gas distribution [2]. The combination of flexibility and resistance makes HDPE superior to other materials for the design of submerged pipeline systems. The installation is often performed by progressively flooding of one of its ends. According to Palacios [3], the advantage of this method is the time required for installation, the

major drawback being the control process of submersion which is a problem due to high curvature to which the pipe is subjected. Moreover, environmental conditions during the pipes lifetime affect the loads supported, as well as stresses and strains.

Computational systems have been used to predict the mechanical behavior of these pipes through nonlinear dynamic analysis. In general, for mechanical behaviour analyses, truss or beam models are adopted. A truss model is computationally cheaper, but less accurate and does not take account of bending stiffness. Instead, a beam model represents satisfactorily problems where bending stiffness should not be overlooked, but its use requires a larger computational effort. In this context, as a first step to simulate the submersion of HDPE pipes, this work aims to develop the formulation of a simplified beam element which has fewer degrees of freedom, but can correctly calculate the geometrical and material nonlinear behaviour.

Alternatives to simplify the beam model have been proposed based on concentrated mass models. An example is the work of Ghadimi [4], who obtained the bending moment from the change of slope between adjacent elements and subsequently calculated equivalent shearing forces from the change of bending moment. The present work is based on the approach of Low and Langley [5], in which the bending stiffness is considered by the contribution of a rotational spring between two adjacent bar elements. These authors obtain the spring rotational stiffness using a potential energy approach, considering some approximations. In this work, the expressions for the internal force vector and tangent stiffness matrix is developed from the principle of virtual work (PTV) and its exact linearization (no approximations), and thus the best possible (quadratic) convergence rate in the solution method is achieved.

Regarding the non-linear solution, implicit and explicit approaches are implemented. In the implicit case, a Newton-Raphson procedure coupled to the Newmark algorithm (average acceleration) is employed, while in the explicit alternative, central differences are adopted. For conciseness, only implicit results are shown in this article. Explicit results are very similar.

Concerning material behavior, polymers are often characterized as viscoelastic or viscoplastic, suggesting a combination of viscous flow, typical of fluids, with plastic or elastic characteristics, typical of solids. Indeed, the challenge in studying and modeling these materials comes from the fact that all these three types of idealized behaviour exist simultaneously in any relative proportion [2]. Studies show that, at room temperature, HDPE has a nonlinear viscoelastic behaviour at any stress level [6]. However, as a first study to model polymeric tubes, this work has its focus in linear viscoelasticity, where the material rheological properties are independent of stress and strain levels, and creep and relaxation functions are only dependent of time. The derivation of the function that models linear viscoelasticity in the bending contribution of simplified beam model is based in the work of Kaliskeand Rothert [7], who present a tridimensional viscoelastic formulation applied to finite element methods and uses generalized Maxwell elements.

The implementation of the simplified beam element presented in this work relies on the modification of the bar element available in program ATENAS 5.0, which is a code developed for academic purposes in UDESC by Muñoz-Rojas and his students. The linear viscoelastic model adopted for the bending contribution is derived from the generalized Maxwell model. On the other hand, the axial viscoelastic contribution already present in ATENAS is modeled based on the generalized Kelvin-Voigt model. Thus, an interconversion between Maxwell and Kelvin viscoelastic properties is needed to ensure consistence when using the input data. This work uses an interconversion for material functions represented by Prony series [8]]. The derivation of the tangent stiffness for the viscoelastic formulation adopts some approximations and does not lead to quadratic convergence. At the same time that this issue demands further development, at the present stage explicit integration in time can already be highly attractive.

2 ATENAS

The implementation of the simplified beam element is performed by modifying the bar element present in program ATENAS 5.0.The formulation used for the geometric nonlinearity in the existent bar element is based on reference [11], although it differs in the sense that it is completely described using interpolation functions and the rotated engineering stress and stress tensors are adopted as a conjugate pair. Starting from the principle of virtual work, an expression for the internal force vector is developed and its exact differentiation yields the tangent stiffness matrix [12]. Regarding the solution procedure, both explicit and implicit methods are implemented. In the former, a central differences scheme is used. In the latter, the code employs average accelerations (Newmark) coupled to the Newton-Raphson method. The linear viscoelastic model implemented for the bar element (axial contribution) is derived from the generalized Kelvin-Voigt model and its formulation is based on references [13] and [14].

3 SIMPLIFIED BEAM ELEMENTS

In this paper, inspired in the work published by Low and Langley [5], bending stiffness is introduced in the bar element by means of rotational springs between two adjacent bar elements. The forces of an equivalent rotational spring are derived directly from the work expression in global coordinates, thus eliminating the need for transformations between local and global coordinate systems. Additionally, the formulation can easily be extended to obtain the consistent stiffness matrix. However reference [5] assumes some approximations to perform the derivatives, which cause loss of convergence rate in the Newton-Raphson method. On the other hand, the present work develops an exact (consistent) tangent stiffness matrix, resulting in quadratic convergence rate in the solution method.

3.1 Bending internal force

Assuming a cable profile initially straight, the strain work W_i, due to the application of an angular displacement θ_i at point i is expressed as

$$W_i = \frac{1}{2} M_i \theta_i. \tag{1}$$

The moment-curvature relationship at an arbitrary point of the beam is given by

$$M_i = EI\kappa, \tag{2}$$

where EI is the bending stiffness, κ is the curvature given by the radius of curvature $R = 1/\kappa$, and θ_i is the bending angle at point i.

Let us take the point i as being located at the node between two adjacent bar elements. An expression for the radius of curvature can be approximated by considering the arc that interpolates three nodes of the elements, as shown in Figure 1. Note that the global node i corresponds to the local node 2 (node corresponding to the rotational spring) and the elements j and k correspond to the elements on the left and right to the spring, respectively.

Using trigonometric properties and the law of cosines, it is possible to equate the expression of the distance between the vertices 1 and 3, generated by the triangle formed by the arc center and vertices 1 and 3, and by the triangle of vertices 1, 2 and 3. Thus, the relationship between the angle between elements (θ_i) and the radius of curvature is given by

$$\theta_i = \frac{1}{2R}\left(L_{oj} + L_{ok}\right), \tag{3}$$

where L_{oj} and L_{ok} are the original lengths of the respective elements j and k. From equation 3 the curvature results in

$$\kappa = \frac{2\theta_i}{\left(L_{oj}+L_{ok}\right)}. \tag{4}$$

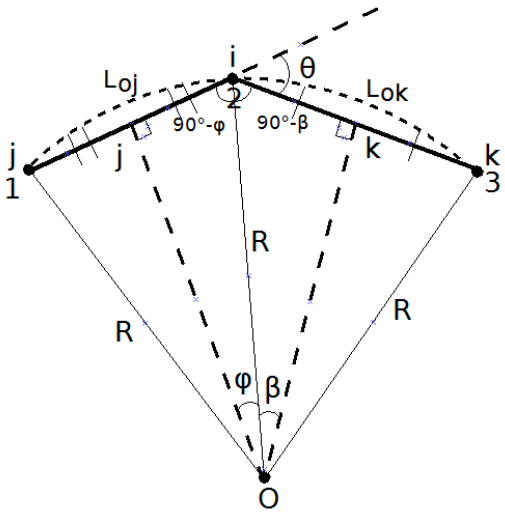

Figure 1 – Arc between elements to find the curvature expression.

Substituting equation 2 and equation 4 into equation 1 yields

$$W_i = \frac{1}{2}k_b\theta_i{}^2, \tag{5}$$

where k_b is the bending stiffness of the spring

$$k_b = \frac{2EI}{\left(L_{oj}+L_{ok}\right)}. \tag{6}$$

Using the principle of virtual work (PTV) and applying a kinematically admissible virtual displacement $\delta\mathbf{u}$ in equation 5, it comes out that

$$\delta W_i = k_b\theta_i \frac{\partial\theta_i}{\partial\mathbf{u}}\delta\mathbf{u} = k_b\theta_i(\delta\mathbf{u})^T\left(\frac{\partial\theta_i}{\partial\mathbf{u}}\right)^T. \tag{7}$$

In order to obtain the derivative $\partial\theta_i/\partial\mathbf{u}$, let's first define vectors **t** and **s**, whose moduli provide the length of elements j and k, respectively,

$$\mathbf{t} = \mathbf{x}_2^S - \mathbf{x}_1^S \tag{8}$$

$$\mathbf{s} = \mathbf{x}_3^S - \mathbf{x}_2^S, \tag{9}$$

where $\mathbf{x}_j^S$ are the global coordinates of node j and the superscript S emphasizes that this node numbering corresponds to the nodes 1-3 associated to the spring. In this case, nodes 1 and 3 correspond to first and last nodes connected to the spring i, and node 2 corresponds to the spring node i (Figure 1). Note that the only nonzero terms in the matrix $\partial\theta_i/\partial\mathbf{u}$ are those corresponding to $\partial\theta_i/\partial\mathbf{u}^S$, so that all the derivation can be done considering only these terms. Hence, for the spring at node i,

$$\mathbf{x}^S = [\mathbf{x}_1^S \quad \mathbf{x}_2^S \quad \mathbf{x}_3^S]^T \tag{10}$$

and

$$\mathbf{x}_k^S = \left[x_k^S \quad y_k^S \quad z_k^S\right]^T, \quad k = 1, 3. \tag{11}$$

Using the definition of scalar product and differentiating with respect to the spring displacement vector, one has

$$\mathbf{t}\cdot\mathbf{s} = |\mathbf{t}||\mathbf{s}|\cos(\theta_i) \tag{12}$$

$$\frac{\partial}{\partial\mathbf{u}^S}(\mathbf{t}\cdot\mathbf{s}) = \frac{\partial}{\partial\mathbf{u}^S}(|\mathbf{t}||\mathbf{s}|\cos(\theta_i)) \tag{13}$$

$$\mathbf{s}^T\frac{\partial\mathbf{t}}{\partial\mathbf{u}^S} + \mathbf{t}^T\frac{\partial\mathbf{s}}{\partial\mathbf{u}^S} = |\mathbf{s}|\cos\theta_i\frac{\partial|\mathbf{t}|}{\partial\mathbf{u}^S} + |\mathbf{t}|\cos\theta_i\frac{\partial|\mathbf{s}|}{\partial\mathbf{u}^S} + |\mathbf{t}||\mathbf{s}|\frac{\partial\cos\theta_i}{\partial\theta_i}\frac{\partial\theta_i}{\partial\mathbf{u}^S}. \tag{14}$$

Noting that

$$\mathbf{t} = \mathbf{x}_2^S - \mathbf{x}_1^S = \mathbf{X}_{21}^S + \mathbf{u}_{21}^S. \tag{15}$$

and denoting as $\mathbb{F}$ the matrix that relates the displacement vector $\mathbf{u}^S$ to the displacements corresponding to the first element, j

$$\mathbf{u}_{21}^S = \begin{bmatrix} -1 & 0 & 0 & 1 & 0 & 0 & 0 & 0 & 0 \\ 0 & -1 & 0 & 0 & 1 & 0 & 0 & 0 & 0 \\ 0 & 0 & -1 & 0 & 0 & 1 & 0 & 0 & 0 \end{bmatrix} \begin{bmatrix} u_1^S \\ v_1^S \\ w_1^S \\ u_2^S \\ v_2^S \\ w_2^S \\ u_3^S \\ v_3^S \\ w_3^S \end{bmatrix} = [\mathbb{F}]\mathbf{u}^S, \tag{16}$$

it turns out that

$$\frac{\partial\mathbf{t}}{\partial\mathbf{u}^S} = \frac{\partial\mathbf{u}_{21}^S}{\partial\mathbf{u}^S} = [\mathbb{F}]. \tag{17}$$

In the same way, differentiating **s** with respect to $\mathbf{u}^S$, results in

$$\frac{\partial\mathbf{s}}{\partial\mathbf{u}^S} = \frac{\partial\mathbf{u}_{32}^S}{\partial\mathbf{u}^S} = [\mathbb{G}], \tag{18}$$

where $\mathbb{G}$ is the matrix that relates the displacement vector $\mathbf{u}^S$ with the displacements corresponding to the second element, k.

Using the definition of the Jacobian, in local element coordinates (now node numbering 1 and 2 correspond to the first and second nodes of element j), and differentiating $|\mathbf{t}|$ with respect to $\mathbf{u}^S$,

$$|\mathbf{t}| = |\mathbf{x_2} - \mathbf{x_1}| = 2J_j(\mathbf{x}) = [-1 \quad 0 \quad 0 \quad 1 \quad 0 \quad 0] \begin{bmatrix} X_1 + u_1 \\ Y_1 + v_1 \\ Z_1 + w_1 \\ X_2 + u_2 \\ Y_2 + v_2 \\ Z_2 + w_2 \end{bmatrix} \tag{19}$$

$$\frac{\partial |\mathbf{t}|}{\partial \mathbf{u}^S} = 2 \frac{\partial J_j(\mathbf{x})}{\partial \mathbf{u_j}} \frac{\partial \mathbf{u_j}}{\partial \mathbf{u}^S} = [-1 \quad 0 \quad 0 \quad 1 \quad 0 \quad 0][\mathbf{T_j}] \tag{20}$$

where $\mathbf{T_j}$ is the rotation matrix for the element j,

$$\mathbf{T_j} = \begin{bmatrix} c_1^1 & c_1^2 & c_1^3 & 0 & 0 & 0 & 0 & 0 & 0 \\ 0 & 0 & 0 & 0 & 0 & 0 & 0 & 0 & 0 \\ 0 & 0 & 0 & 0 & 0 & 0 & 0 & 0 & 0 \\ 0 & 0 & 0 & c_1^1 & c_1^2 & c_1^3 & 0 & 0 & 0 \\ 0 & 0 & 0 & 0 & 0 & 0 & 0 & 0 & 0 \\ 0 & 0 & 0 & 0 & 0 & 0 & 0 & 0 & 0 \end{bmatrix}, \tag{21}$$

and c_1^k is the direction cosine of the local axis 1 (x) with respect to the k-th global axis (1, 2 and 3, corresponding to x^G, y^G and z^G). Hence,

$$\frac{\partial |\mathbf{t}|}{\partial \mathbf{u}^S} = [-c_1^1 \quad -c_1^2 \quad -c_1^3 \quad c_1^1 \quad c_1^2 \quad c_1^3 \quad 0 \quad 0 \quad 0] = \mathbf{c_{1J}^T}[\mathbb{F}] = [\mathbb{L}], \tag{22}$$

where $\mathbf{c_{1J}}$ and $\mathbb{L}$ are the vector and matrix formed by the direction cosines for element j.

By analogy, using the definition of the Jacobian in local element coordinates and differentiating $|\mathbf{s}|$ with respect to $\mathbf{u}^S$, leads to

$$\frac{\partial |\mathbf{s}|}{\partial \mathbf{u}^S} = [0 \quad 0 \quad 0 \quad -c_1^1 \quad -c_1^2 \quad -c_1^3 \quad c_1^1 \quad c_1^2 \quad c_1^3] = \mathbf{c_{1k}^T}[\mathbb{G}] = [\mathbb{N}] \tag{23}$$

where $\mathbf{c_{1k}}$ and $\mathbb{N}$ are the vector and matrix formed by the direction cosines for element k.

Substituting the expressions computed above in equation 14, the expression for $\partial\theta_i/\partial\mathbf{u}^S$ is obtained as

$$\frac{\partial \theta_i}{\partial \mathbf{u}^S} = -\frac{1}{|\mathbf{t}||\mathbf{s}| \sin\theta_i} \{\mathbf{s^T}[\mathbb{F}] + \mathbf{t^T}[\mathbb{G}] - (|\mathbf{s}|[\mathbb{L}] + |\mathbf{t}|[\mathbb{N}]) \cos\theta_i\}. \tag{24}$$

Using the PTV, given by the previous expression and equation 7, leads to

$$\delta W_i = (\delta \mathbf{u}^S)^T \mathbf{q}^S = (\delta \mathbf{u}^S)^T k_b \theta_i \left(\frac{\partial \theta_i}{\partial \mathbf{u}^S}\right)^T. \tag{25}$$

In this expression $\mathbf{q}^S$ is the bending internal force vector for each spring. Using the equality

$$\mathbf{q}^S = k_b \theta_i \left(\frac{\partial \theta_i}{\partial \mathbf{u}^S}\right)^T, \tag{26}$$

it finally results in

$$\mathbf{q}^{\mathrm{S}} = -\frac{k_b \theta_i}{|\mathbf{t}||\mathbf{s}| \sin\theta_i}\{[\mathbb{F}]^{\mathrm{T}}\mathbf{s} + [\mathbb{G}]^{\mathrm{T}}\mathbf{t} - (|\mathbf{s}|[\mathbb{L}]^{\mathrm{T}} + |\mathbf{t}|[\mathbb{N}]^{\mathrm{T}})\cos\theta_i\}. \tag{27}$$

3.2 Bending tangent stiffness matrix

Using the spring nodal numbering, the bending tangent stiffness matrix for each rotational spring (order 9) can be defined as

$$\mathbf{k}^{\mathrm{S}} = \frac{\partial \mathbf{q}^{\mathrm{S}}}{\partial \mathbf{u}^{\mathrm{S}}}. \tag{28}$$

In order to simplify the presentation of the mathematical development, the tangent stiffness matrix will be separated into two terms, $\mathbf{k}_1^{\mathrm{S}}$ and $\mathbf{k}_2^{\mathrm{S}}$,

$$\mathbf{k}_1^{\mathrm{S}} = -([\mathbb{F}]^{\mathrm{T}}\mathbf{s} + [\mathbb{G}]^{\mathrm{T}}\mathbf{t} - (|\mathbf{s}|[\mathbb{L}]^{\mathrm{T}} + |\mathbf{t}|[\mathbb{N}]^{\mathrm{T}})\cos\theta_i)\frac{\partial}{\partial \mathbf{u}^{\mathrm{S}}}\left(\frac{k_b \theta_i}{|\mathbf{t}||\mathbf{s}| \sin\theta_i}\right). \tag{29}$$

$$\mathbf{k}_2^{\mathrm{S}} = -\frac{k_b \theta_i}{|\mathbf{t}||\mathbf{s}| \sin\theta_i}\frac{\partial}{\partial \mathbf{u}^{\mathrm{S}}}([\mathbb{F}]^{\mathrm{T}}\mathbf{s} + [\mathbb{G}]^{\mathrm{T}}\mathbf{t} - (|\mathbf{s}|[\mathbb{L}]^{\mathrm{T}} + |\mathbf{t}|[\mathbb{N}]^{\mathrm{T}})\cos\theta_i). \tag{30}$$

Using differentiation rules, expanding the terms and using expressions previously calculated, leads to 6 terms of the tangent stiffness matrix for each spring

$$\mathbf{k}^{\mathrm{S}} = \mathbf{k}_{\mathbf{1A}}^{\mathrm{S}} + \mathbf{k}_{\mathbf{1B}}^{\mathrm{S}} + \mathbf{k}_{\mathbf{2A}}^{\mathrm{S}} + \mathbf{k}_{\mathbf{2B}}^{\mathrm{S}} + \mathbf{k}_{\mathbf{2C1}}^{\mathrm{S}} + \mathbf{k}_{\mathbf{2C2}}^{\mathrm{S}}, \tag{31}$$

where

$$\mathbf{k}_{\mathbf{1A}}^{\mathrm{S}} = \frac{k_b}{\sin\theta_i}(\sin\theta_i - \theta_i\cos\theta_i)\left(\frac{\partial\theta_i}{\partial \mathbf{u}^{\mathrm{S}}}\right)^{\mathrm{T}}\left(\frac{\partial\theta_i}{\partial \mathbf{u}^{\mathrm{S}}}\right), \tag{32}$$

$$\mathbf{k}_{\mathbf{1B}}^{\mathrm{S}} = -\frac{k_b \theta_i}{|\mathbf{t}||\mathbf{s}|}\left(\frac{\partial\theta_i}{\partial \mathbf{u}^{\mathrm{S}}}\right)^{\mathrm{T}}(|\mathbf{s}|[\mathbb{L}] + |\mathbf{t}|[\mathbb{N}]), \tag{33}$$

$$\mathbf{k}_{\mathbf{2A}}^{\mathrm{S}} = -\frac{k_b \theta_i}{|\mathbf{t}||\mathbf{s}| \sin\theta_i}([\mathbb{F}]^{\mathrm{T}}[\mathbb{G}] + [\mathbb{G}]^{\mathrm{T}}[\mathbb{F}]), \tag{34}$$

$$\mathbf{k}_{\mathbf{2B}}^{\mathrm{S}} = -\frac{k_b \theta_i}{|\mathbf{t}||\mathbf{s}|}(|\mathbf{s}|[\mathbb{L}]^{\mathrm{T}} + |\mathbf{t}|[\mathbb{N}]^{\mathrm{T}})\frac{\partial\theta_i}{\partial \mathbf{u}^{\mathrm{S}}}, \tag{35}$$

$$\mathbf{k}_{\mathbf{2C1}}^{\mathrm{S}} = \frac{k_b \theta_i \cos\theta_i}{|\mathbf{t}||\mathbf{s}| \sin\theta_i}([\mathbb{L}]^{\mathrm{T}}[\mathbb{N}] + [\mathbb{N}]^{\mathrm{T}}[\mathbb{L}]), \tag{36}$$

$$\mathbf{k}_{\mathbf{2C2}}^{\mathrm{S}} = \frac{k_b \theta_i \cos\theta_i}{|\mathbf{t}||\mathbf{s}| \sin\theta_i}\left(\frac{|\mathbf{s}|}{|\mathbf{t}|}[\mathbb{F}]^{\mathrm{T}}\left([\mathbb{F}] - \mathbf{c}_{\mathbf{1J}}[\mathbb{L}]\right) + \frac{|\mathbf{t}|}{|\mathbf{s}|}[\mathbb{G}]^{\mathrm{T}}([\mathbb{G}] - \mathbf{c}_{\mathbf{1K}}[\mathbb{N}])\right). \tag{37}$$

The implementation uses a mapping to relate the positions of the bending stiffness matrix and internal force vector for each spring to the respective degrees of freedom in the global system. To obtain internal forces and corresponding stiffness matrices, the contributions of axial and bending forces are added in their respective global degrees of freedom.

4 LINEAR VISCOELASTIC MODEL

The derivation of the linear viscoelastic material function for the simplified beam element is based on reference [7], which presents a tridimensional viscoelastic formulation applied to finite element computations and uses generalized Maxwell elements.

Replacing equation 4 in the moment-curvature relationship (equation 2), results in a relationship between the moment and angle between the beam elements,

$$M_i = k_b \theta_i = \frac{2EI\theta_i}{(L_{oj}+L_{ok})}, \tag{38}$$

where M_i is the moment acting on a node, E is the modulus of elasticity, I is the moment of inertia, L_{oj} and $L_{ok}$are the lengths of the elements before and after node i, respectively, and θ_i is the angle between the elements. Assuming no change in the cross section along the axis length and considering small extensional deformations, the above equation results in

$$M_i = \mathbb{C}_i E \theta_i, \tag{39}$$

where $\mathbb{C}_i = \frac{2I}{(L_{oj}+L_{ok})}$is constant.

From the stress-strain relationship for linear viscoelastic materials (equation 40), by analogy to the moment-angle relationship, it comes out that

$$\sigma(t) = E(t)\varepsilon_c \tag{40}$$

$$M_i(t) \sim \sigma(t) \tag{41}$$

$$\theta_i \sim \varepsilon_c \tag{42}$$

so that

$$M_i(t) = \mathbb{C}_i E(t) \theta_i. \tag{43}$$

According to reference [2], linear viscoelasticity can be represented by

$$\sigma(t) = \int_0^t E(t-s)\frac{\partial \varepsilon(s)}{\partial s} ds. \tag{44}$$

From this point on, the index representing node i is omitted in favor of neatness in the text presentation. The development of the numerical model starts from the integral representation of linear viscoelasticity (equation 44), using the analogy to the moment

$$M(t) = \int_0^t \mathbb{C} E(t-s)\frac{\partial \theta(s)}{\partial s} ds, \tag{45}$$

where

$$E(t-s) = E_e + \sum_{j=1}^{m} E_j e^{\left(-\frac{t-s}{\rho_j}\right)} \tag{46}$$

where m is the number of Maxwell elements. Splitting equation 45 into elastic and viscoelastic parts results in

$$M(t) = \int_0^t \mathbb{C}E_e \frac{\partial\theta(s)}{\partial s} ds + \int_0^t \sum_{j=1}^m \mathbb{C}E_j e^{\left(-\frac{t-s}{\rho_j}\right)} \frac{\partial\theta(s)}{\partial s} ds\,, \tag{47}$$

$$M(t) = \mathbb{C}E_e\theta(t) + \sum_{j=1}^m \int_0^t \mathbb{C}E_j e^{\left(-\frac{t-s}{\rho_j}\right)} \frac{\partial\theta(s)}{\partial s} ds, \tag{48}$$

$$M(t) = M_e(t) + \sum_{j=1}^m h_j(t), \tag{49}$$

where $M_e(t)$ is the elastic component of the response. The goal of the next steps is to obtain an efficient numerical formulation for the solution of the integral $h_j(t)$. In analogy to the development in reference [7], the following recursive formula is obtained

$$h_j^{n+1} = e^{\left(-\frac{\Delta t}{\rho_j}\right)} h_j^n + \mathbb{C}E_j \frac{1 - e^{\left(-\frac{\Delta t}{\rho_j}\right)}}{\frac{\Delta t}{\rho_j}} [\theta^{n+1} - \theta^n]. \tag{50}$$

The final equation for the moment considering linear viscoelasticity is given by

$$M^{n+1} = \mathbb{C}E_e\theta^{n+1} + \sum_{j=1}^m h_j{}^{n+1}. \tag{51}$$

In the simplified beam element formulation deduced previously, the internal force vector in each spring is given by

$$\mathbf{q}^S = k_b\theta \frac{\partial\theta}{\partial \mathbf{u}^S}. \tag{52}$$

Substituting equation 38 it follows that

$$\mathbf{q}^S = M \frac{\partial\theta}{\partial \mathbf{u}^S}. \tag{53}$$

Applying the viscoelastic model, the internal force vector associated to the spring at node i is finally given by

$$\left(\mathbf{q}_V^S\right)^{n+1} = \left[\mathbb{C}E_e\theta^{n+1} + \sum_{j=1}^m h_j{}^{n+1}\right] \frac{\partial\theta^{n+1}}{\partial\left(\mathbf{u}^S\right)^{n+1}}, \tag{54}$$

Correspondingly, the tangent bending stiffness matrix is given by differentiation of the internal force,

$$\left(\mathbf{k}_V^S\right)^{n+1} = \frac{\partial\left(\mathbf{q}_V^S\right)^{n+1}}{\partial\left(\mathbf{u}^S\right)^{n+1}} \tag{55}$$

Clearly, in the differentiation of $\mathbf{q}_V^S$, θ^{n+1} is the only variable dependent on displacements. Thus, replacing equations 54, 50 and 52 in 55, the derivative yields the tangent bending stiffness matrix for the viscoelastic model

$$\left(\mathbf{k}_{\mathbf{V}}^{\mathrm{S}}\right)^{\mathrm{n+1}} = \left(\mathbb{C}\mathrm{E}_{\mathrm{e}} + \sum_{\mathrm{j=1}}^{\mathrm{m}} \mathbb{C}\mathrm{E}_{\mathrm{j}} \frac{1-\mathrm{e}^{\left(-\frac{\Delta \mathrm{t}}{\rho_{\mathrm{j}}}\right)}}{\frac{\Delta \mathrm{t}}{\rho_{\mathrm{j}}}} \right) \frac{1}{k_b} \left(\mathbf{k}^{\mathrm{S}}\right)^{\mathrm{n+1}} \tag{56}$$

where $\mathbf{k}^{\mathrm{S}}$ and $\mathbf{k}_{\mathbf{V}}^{\mathrm{S}}$ are the stiffness matrices for the simplified elastic and viscoelastic beam models, respectively.

4.1 Interconversion between viscoelastic functions

The main reason to perform an interconversion in this work is that the viscoelastic model implemented in ATENAS for the bar element requires creep constants $\mathrm{D_i}$, which are associated to the generalized Kelvin-Voigt model, whereas the simplified viscoelastic bending contribution requires relaxation constants $\mathrm{E_j}$, which are associated to the generalized Maxwell model. Hence, a function interconversion is needed so that the code input data (creep constants) can be internally converted to represent the same material for each element. The numerical interconversion used in this work considers linear viscoelastic material functions based on representations via Prony series [8][10].

4.1.1 Relaxation Modulus from creep compliance

It can be shown that for a unit strain, the relationship between the relaxation modulus E(t) and the creep compliance D(t) is given by [8],

$$\int_0^{\mathrm{t}} \mathrm{D}(\mathrm{t}-\tau) \frac{\mathrm{dE}(\tau)}{\mathrm{d}\tau} \mathrm{d}\tau = 1. \tag{57}$$

The Prony series representation of the relaxation modulus E(t), is described by

$$\mathrm{E}(\mathrm{t}) = \mathrm{E_e} + \sum_{\mathrm{i=1}}^{\mathrm{N}} \mathrm{E_i} \mathrm{e}^{\frac{-\mathrm{t}}{\rho_{\mathrm{i}}}}. \tag{58}$$

and the Prony series representation of creep compliance D(t) is given by

$$\mathrm{D}(\mathrm{t}) = \mathrm{D_e} + \sum_{\mathrm{i=1}}^{\mathrm{N}} \mathrm{D_i} \left(1 - \mathrm{e}^{\frac{-\mathrm{t}}{\tau_{\mathrm{i}}}}\right). \tag{59}$$

In order to obtain the derivative of the relaxation module, its representation must include the sudden application, using the concept of a unit step function due to the discontinuity at $\tau = 0$,

$$\mathrm{E}(\mathrm{t}) = \mathrm{H}(\mathrm{t}) \left[\mathrm{E_e} + \sum_{\mathrm{i=1}}^{\mathrm{m}} \mathrm{E_i} \mathrm{e}^{\left(\frac{-\mathrm{t}}{\rho_{\mathrm{i}}}\right)} \right], \tag{60}$$

where H(t) is the Heaviside function.

Using the chain rule of differentiation, where $\delta(\tau)$ is the Dirac delta function, the derivative is given by

$$\frac{\mathrm{dE}(\mathrm{t})}{\mathrm{d}\tau} = \delta(\tau) \left[\mathrm{E_e} + \sum_{\mathrm{i=1}}^{\mathrm{m}} \mathrm{E_i} \mathrm{e}^{\left(\frac{-\tau}{\rho_{\mathrm{i}}}\right)} \right] + \mathrm{H}(\tau) \left[\sum_{\mathrm{i=1}}^{\mathrm{m}} -\frac{\mathrm{E_i}}{\rho_{\mathrm{i}}} \mathrm{e}^{\left(\frac{-\tau}{\rho_{\mathrm{i}}}\right)} \right]. \tag{61}$$

Replacing equations 59 and 61 in equation 57, results in

$$\int_0^t \left[D_e + \sum_{j=1}^{n} D_j \left(1 - e^{\frac{-(t-\tau)}{\tau_j}} \right) \right] \left\{ \delta(\tau) \left[E_e + \sum_{i=1}^{m} E_i e^{\left(\frac{-\tau}{\rho_i}\right)} \right] + H(\tau) \left[\sum_{i=1}^{m} -\frac{E_i}{\rho_i} e^{\left(\frac{-\tau}{\rho_i}\right)} \right] \right\} d\tau = 1 \qquad (62)$$

After some algebra, the equations that perform the relaxation modulus interconversion, having creep compliance as input data, are described by the following matrix equation [9]:

$$A_{ki} E_i = B_k, \qquad (63)$$

where

$$A_{ki} = \begin{cases} -D_e \left(1 - e^{\frac{-t_k}{\rho_i}} \right) + \sum_{j=1}^{n} \left(-D_j \left(1 - e^{\frac{-t_k}{\rho_i}} \right) + \frac{\tau_j D_j}{\tau_j - \rho_i} \left(e^{\frac{-t_k}{\tau_j}} - e^{\frac{-t_k}{\rho_i}} \right) \right) & \text{se } \rho_i \neq \tau_j \\ -D_e \left(1 - e^{\frac{-t_k}{\rho_i}} \right) + \sum_{j=1}^{n} \left(-D_j \left(1 - e^{\frac{-t_k}{\rho_i}} \right) + \frac{D_j}{\rho_i} t_k e^{\frac{-t_k}{\tau_j}} \right) & \text{se } \rho_i = \tau_j \end{cases} \qquad (64)$$

and

$$B_j = 1 - \frac{\left[D_e + \sum_{j=1}^{n} D_j \left(1 - e^{\frac{-t_k}{\tau_j}} \right) \right]}{D_e}. \qquad (65)$$

D_e, D_j, ρ_i (i = 1, ..., m), τ_j (j = 1, ..., n) and t_k (k = 1, ..., p) are known or stipulated variables.

The solution of the system of linear equations (equation 63) requires the collocation method when p = m and the least squares method when p> n [8].

In the case of the collocation method, t_k should be adopted as $t_k = a\tau_j$ where, according to reference [9], the constant "a" must assume values between 2 and 5. Outside this range, numerical instability problems are likely to occur, resulting in negative terms in the Prony series for E(t). Furthermore, a first approximation to the time constants for relaxation modulus ρ_i can be obtained imposing ρ_i equal to the time constants for creep compliance τ_j.

5 VALIDATION AND EXAMPLES

5.1 Tangent stiffness matrix

In this study the exact expression for the bending tangent stiffness matrix is developed by differentiation of the internal force with respect to nodal displacements. A comparison to the numerical tangent stiffness matrix is made to verify if the calculated matrix is correct. The numerical matrix is calculated using central finite difference, as represented in equation 66,

$$K_{ij} = \frac{\partial q_i}{\partial u_j} = \frac{q_i(u_j + \Delta u) - q_i(u_j - \Delta u)}{2\Delta u_j}, \qquad (66)$$

where the internal force q_i is given by imposing a small displacement Δu in the degree of freedom j. The displacement applied must be sufficiently small so that the expression results in a derivative approximation rather than in a secant. On the other hand, it must be large enough to avoid large numerical errors associated to the computer's finite precision.

Several comparison tests are conducted to compare the two matrices, showing negligible error in the elastic case. On the other hand, due to some approximations adopted in the derivation of the viscoelastic tangent stiffness, differences between the analytical and numerical matrices occurred.

5.2 Residue convergence rate

If the tangent matrix is obtained by calculating the exact derivative, the implementation of the NR method should result in quadratic convergence near the roots. This means that each new residue should be proportional to the square of the previous one.

Several examples are tested and the residue is verified in each iteration. As expected (in view of Section 5.1), quadratic convergence is obtained for all examples for the elastic material model. Table 1 presents the residue convergence for a given load step in a typical elastic beam problem using this formulation. The convergence rate for the values in the Table is approximately 2.3.

Table 1 – Residue in each iteration, Newton-Rapson method.

Iteration	**Residue**
1	1.00000×10^{0}
2	9.47359×10^{-1}
3	2.16870×10^{-2}
4	5.40335×10^{-6}
5	1.9880×10^{-14}

5.3 Simplified beam model – Small displacements

For a first validation of the simplified beam element, two examples involving small displacements and strains are analyzed. In this case, if only bending stiffness is considered, the solution should agree with the Euler-Bernoulli beam equation. Two load cycles are applied considering damping proportional to the lumped mass. In the first cycle the load is applied quickly while in the second the load is kept until stabilization of displacements. The accuracy of results is evaluated, using 10 and 40 elements in each of the examples. The data for both problems is presented in Table 2.

Table 2 – Data of examples for the simplified beam model.

Problem data	
Proportional Damping	5
Diameter of the cross-section	60 mm
Density	7860.0 Kg/m³
Young modulus	210.0×10^{9} N/m^2

5.3.1 Example 1 - Bi-supported elastic beam

The geometric definition of this example is shown in Figure 2. Note that both ends are constrained in horizontal and vertical directions. The entire length of the beam is divided in elements of equal size, using 10 and 40 elements. A force of 6000N is applied at the mid-length of the beam, resulting in small displacements.

Due to symmetry, Figure 3(a) shows the vertical displacement at each node only along half length. The curves show the results obtained with the implementation developed in this study and those predicted by Euler-Bernoulli theory. In Fig. 3(b), errors relative to the Euler-Bernoulli equation are presented. Good agreement is found.

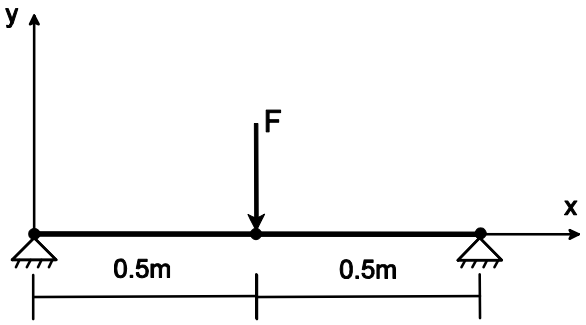

Figure 2 - Example 1 - Bi-supported elastic beam.

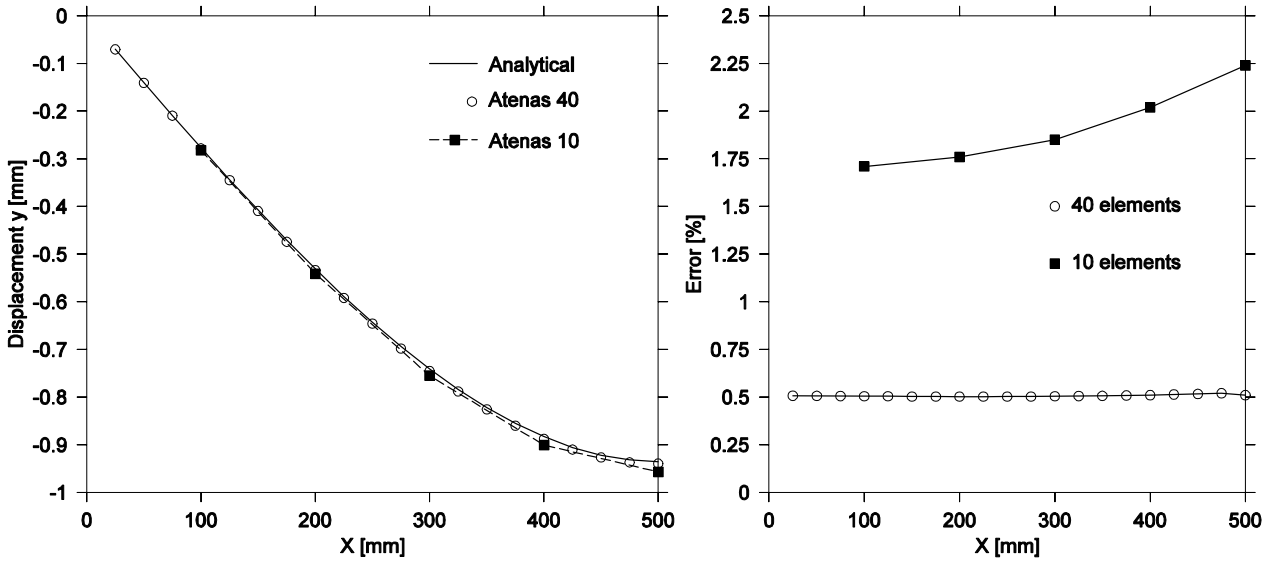

(a) (b)

Figure 3 - Bi-supported elastic beam, only bending stiffness: (a) displacements in y and(b) errors relative to the Euler-Bernoulli equation.

5.3.2 Example 2 – Clamped beam

The geometric definition of this example is given in Figure 4(a). In order to simulate adequately the orthogonality of the elastic curve at the clamped end, an additional element (element zero) with the same length of element 1 is introduced. In each load step (or time increment) its coordinates are updated to be symmetrical to those of the first element, creating a symmetrical point in node 1, Figure 4(b). This way it is possible to enforce zero curvature in the clamped end. The force applied in this problem is 800N.

Figure 5(a) shows the vertical displacement at each node obtained with the implementation developed in this study and according to the Euler-Bernoulli theory. In Fig. 5(b), errors relative to the Euler-Bernoulli equation are presented. As in the previous example, excellent agreement is verified.

5.4 Simplified beam model – Large displacements

In this Section, the formulation of the simplified beam element developed is tested with respect to large displacements. To this end, axial and bending stiffness are coupled, and the solution

is validated against the commercial finite element software Msc Marc. Two load cycles are applied considering damping proportional to the lumped mass. In the first cycle the load is applied quickly, while in the second the load is kept until stabilization of displacements. The accuracy of results is analyzed for discretizations using 10 and 40 elements in each of the examples. The data of the problems is presented in Table 2.

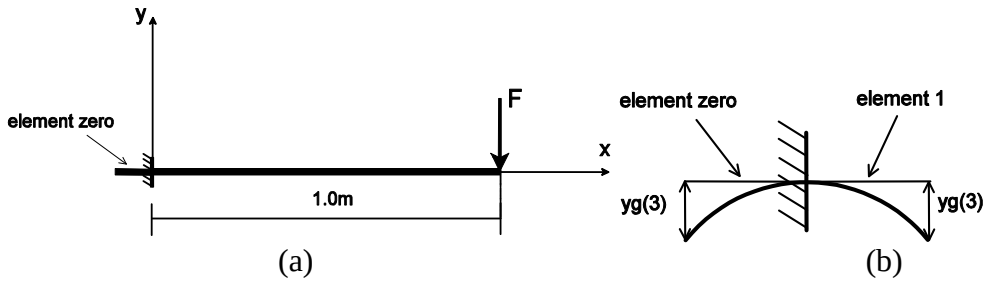

Figure 4 - (a) Example 2 – Clamped beam, (b) Modeling of clamped boundary condition.

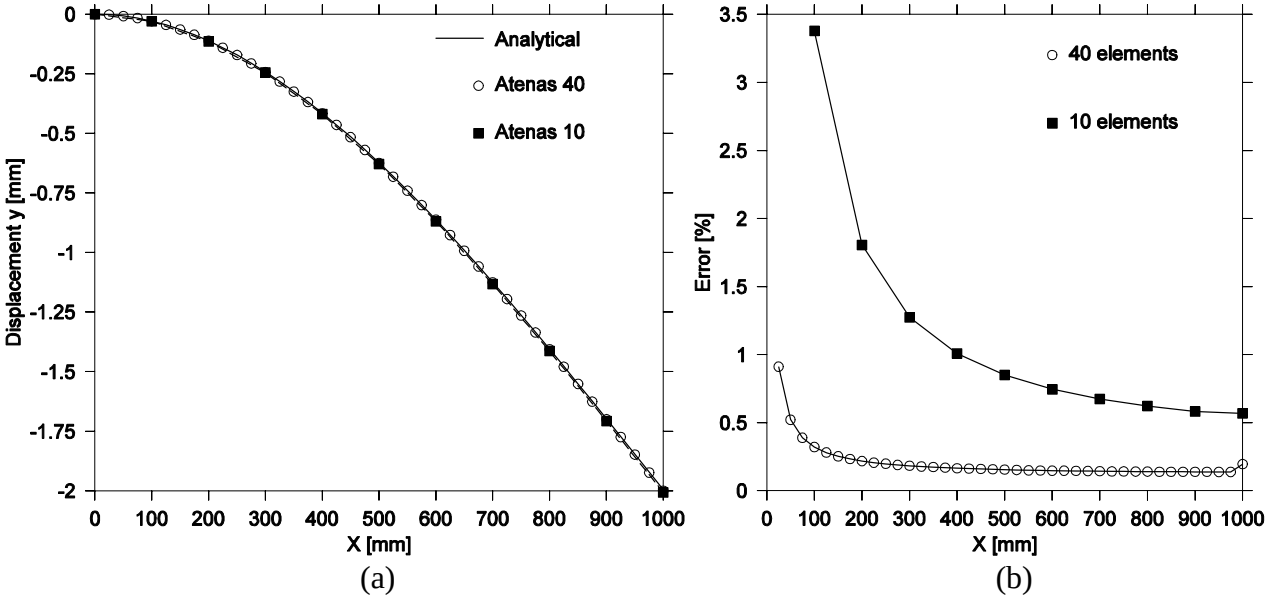

Figure 5–Clamped elastic beam, just bending components: (a) displacements in y and (b) errors relative to the Euler-Bernoulli equation.

5.4.1 Example 1 - Bi-supported elastic beam

The geometric definition of this example is depicted in Figure 2. The entire length is divided into 10 and 40 equal elements.

Considering only half length due to symmetry, Figure 6(a) shows the vertical displacement at each node. Results are obtained according to the present implementation in program ATENAS and to the commercial code Msc Marc. A point load of 6.0×10^5N applied at the mid-length of the beam leads to displacements that require a nonlinear geometric analysis. The Euler-Bernoulli analytical solution is no longer satisfactory in this case. Note that compared to the results provided by Msc Marc, the errors obtained are smaller than 1.1% (10 elements) and 0.3% (40 elements).

5.4.2 Example 2 – Clamped beam

The geometric definition of this example is presented in Figure 4. Figure 7(a) shows the vertical displacement at each node obtained according to the formulation proposed in this work and to the commercial software Msc Marc. A point load of 4.0×10^4 N is applied, leading to displacements that require a nonlinear geometric analysis.

Figure 7(b) shows that, in comparison to the results given by Msc Marc, the error obtained is smaller than 4% and 3.5% next to the boundary condition and around 1% and 0.25% in the last node, for discretizations with 10 and 40 elements, respectively. The boundary condition region has larger errors due to the larger curvature in that neighborhood.

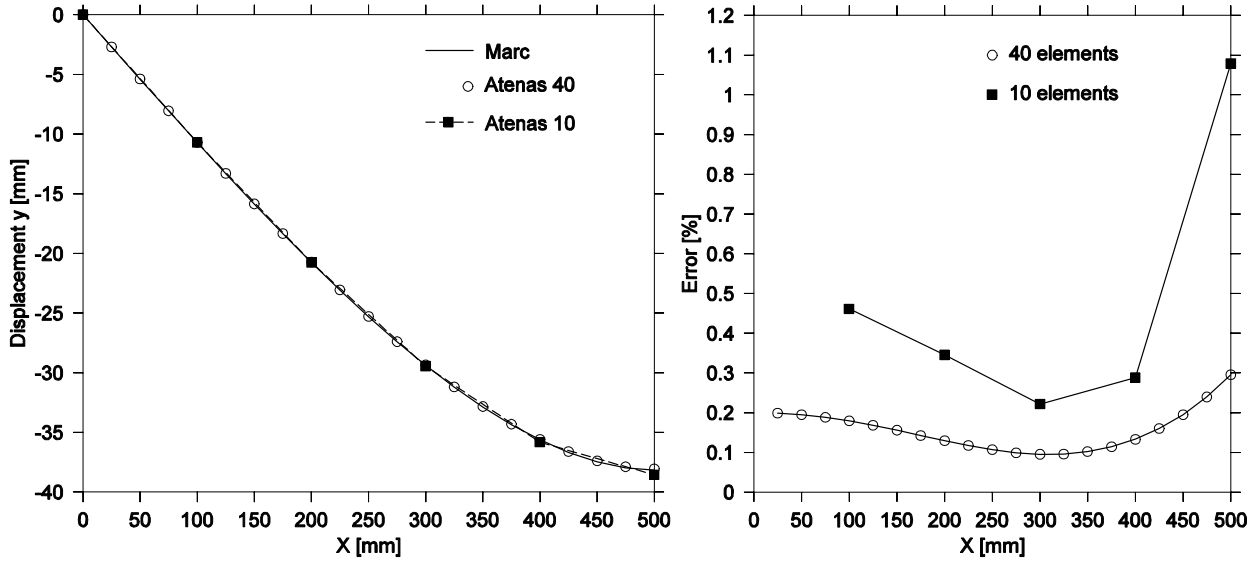

(a) (b)

Figure 6 - Bi-supported elastic beam: (a) displacements in y and (b) errors relative to Msn Marc.

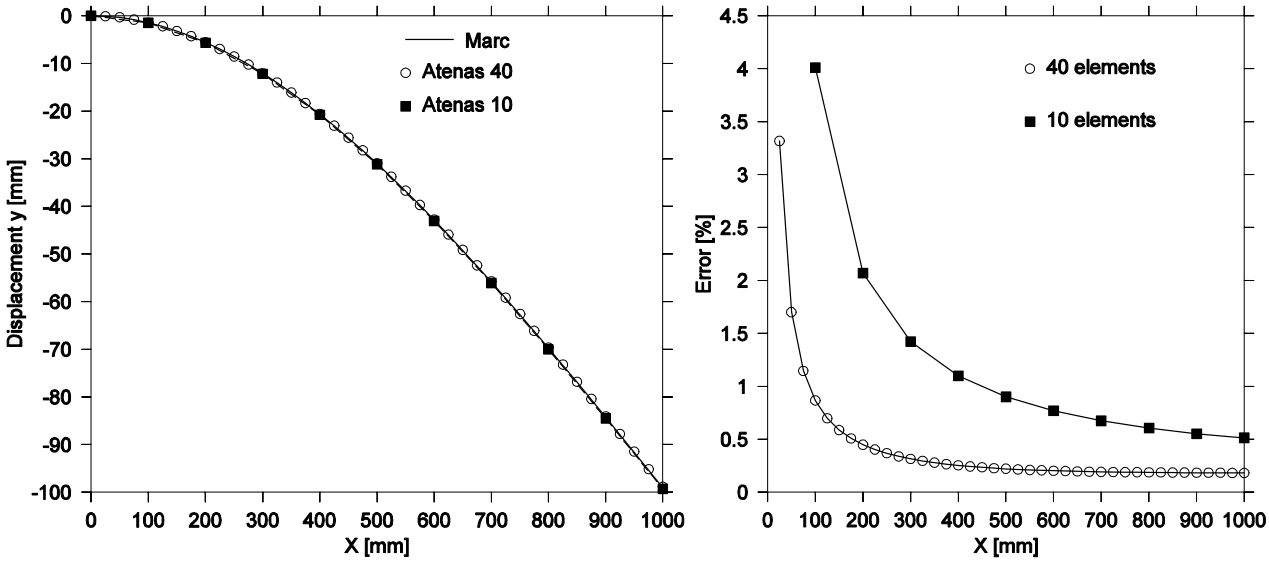

(a) (b)

Figure 7– Clamped elastic beam:(a) displacements in y and (b) errors relative to Msc Marc.

5.5 Transient analysis

The same examples studied for the static analyses are adopted to evaluate the transient response obtained when using the simplified beam model. The displacements obtained via the present formulation are compared to those obtained using the commercial finite element software Msc Marc.

The data of the problems is presented in Table 2, except for damping information, which is not considered in this Section.

5.5.1 Example 1 - Bi-supported elastic beam

The geometric definition of this example is shown in Figure 2. The entire length of the beam is divided into 40 equal elements. A force of 10^6N is applied in ramp up to 10^{-5}s, with time increments of 10^{-7}s. Next the force is kept constant and the viscoelastic response is evaluated at time increments of 2.68×10^{-5}s.

Figure 8(a) depicts a graph showing the vertical displacement at the node where the load is applied against time. The results obtained in ATENAS and Msc Marc are displayed, showing excellent agreement.

5.5.2 Example 2 – Clamped elastic beam

The geometric definition of this example is given in Figure 4. The entire length is divided into 40 equal elements. In this example the force is applied in a ramp from zero to 10^5 N with time increments of 10^{-7}s. Thereafter, time increments of 5.34×10^{-6} s are applied keeping the force constant. The same incrementation is adopted in Marc and ATENAS.

Figure 8(b) shows the vertical displacement at the loaded node versus time obtained in ATENAS and Marc. Good agreement of results is obtained.

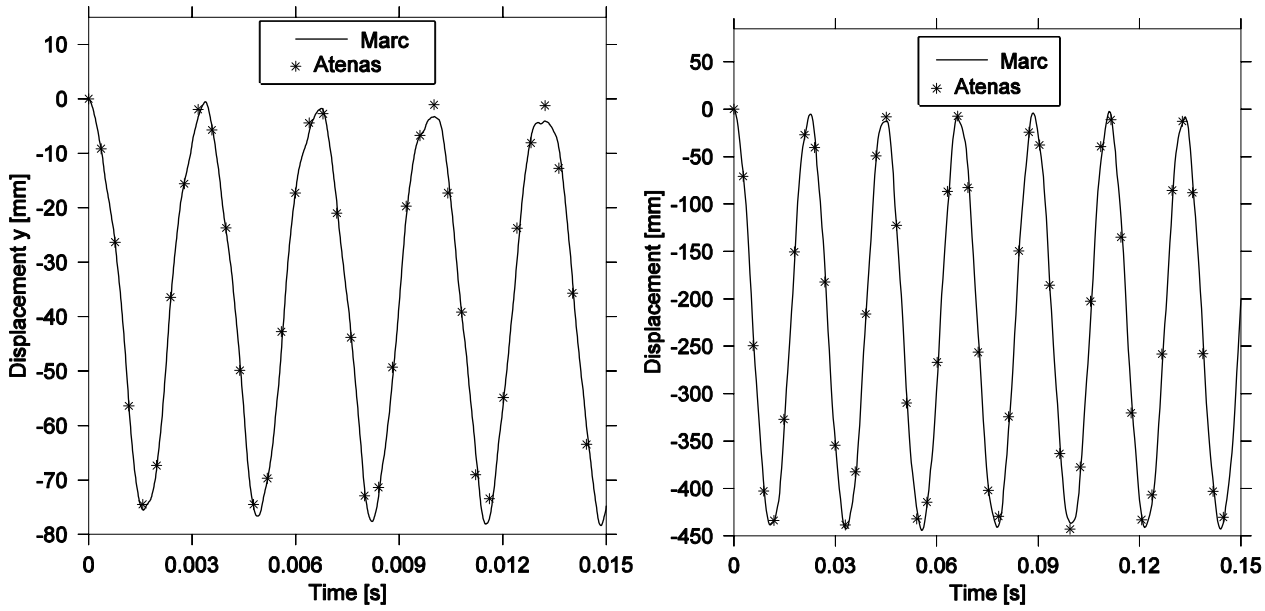

(a) (b)

Figure 8 - Comparison between ATENAS and Marc. (a)bi-supported beam and(b) clamped beam.

5.6 Simplified beam model with linear viscoelasticity

After validating the simplified beam model for static and transient elastic analyses including geometric nonlinearity, the viscoelastic formulation proposed in Section 4 is evaluated using the commercial finite element software Msc Marc as reference again. Once more, a clamped and a bi-supported example are studied, now including material rate dependence. For both cases, two load cycles are imposed. In the first cycle the load is applied quickly (10^{-5}s). In the second cycle, force is kept constant until stabilization of displacements.

The input constants for the Prony series correspond to the generalized Kelvin-Voigt model and refer to examples studied by Brinson and Brinson in reference [10]. These constants represent a linear viscoelastic polymer and are shown in Table 3. Kelvin-Voigt model constants are used as input data because the bar element previously available in ATENAS adopted this mechanical analogy. As the implemented viscoelastic bending contribution is based on the generalized Maxwell model, the constants are converted by the method described in Section 4.1.1. The values obtained are presented in Table 3. The interconversion procedure considers a collocation coefficient equal to 3, and $\rho = \tau$.

In the examples presented in this Section, the specific mass of the beam is 7.339×10^{6} kg/m^3 and the cross section is circular with a diameter of 30 mm.

Table 3 - Prony Constants of a linear viscoelastic polymer.

τ [s]	**Creep Compliance** [mm^2/N]	**Relaxation Modulus** [N/mm^2]
	$D_e = 0.10\times10^{-3}$	$E_e = 5000.0$
0.6	0.207×10^{-4}	1971.06
6	0.318×10^{-4}	1598.30
60	0.231×10^{-4}	837.07
210	0.166×10^{-4}	393.55
600	0.569×10^{-5}	120.49
2100	0.996×10^{-6}	24.20
6000	0.425×10^{-6}	10.39
60000	0.236×10^{-6}	5.92
600000	0.200×10^{-6}	5.02

5.6.1 Example 1 - Bi-supported viscoelastic beam

The geometric definition of this example is depicted in Figure 2. The entire length of the beam is divided into 40 equal elements. In this example the force is applied in a ramp from zero to 10^4 N, with time increments of10^{-5} s. Thereafter, the force is kept constant and time increments of 8.35×10^{-4} s are imposed. The same incrementation is adopted in ATENAS and Marc.

Figure 9(a) shows the vertical displacement at the central node (where the load is applied) versus time, obtained via both programs.

5.6.2 Example 2 – Clamped viscoelastic beam

The geometric definition of this example is displayed in Figure 4. The entire length of the beam is divided into 40 equal elements. The force is applied in a ramp from zero to 100 N with time increments of 10^{-5}s. Thereafter, the force is kept constant and time increments of 7.51×10^{-4}sare imposed. The same incrementation is used in ATENAS and Marc.

Figure 9(b) shows the vertical displacement at the last node (where the load is applied) versus time, obtained in both programs.

Figure 9 shows that excellent agreement between ATENAS and Msc Marc is achieved in both examples, for clamped and bi-supported beams.

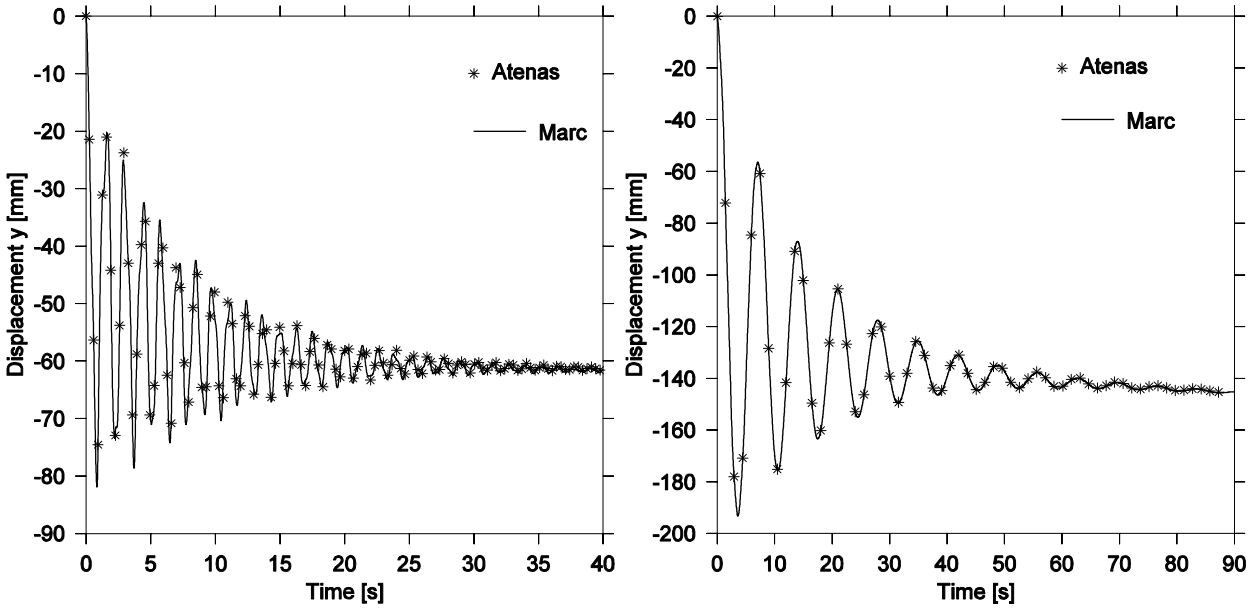

(a) (b)

Figure 9 - (a) Displacement of central node by time, bi-supported beam, (b) Displacement of the last node by time, clamped beam.

6 CONCLUSIONS

Aiming at the analysis of submerged HDPE pipelines, a nonlinear simplified beam element is developed. The formulation retains only translational degrees of freedom (three degrees of freedom per node in a 3D analysis), and is able to simulate correctly the geometric and material nonlinear behavior of a traditional Euler-Bernoulli beam element. Bending stiffness is introduced via rotational springs between two adjacent geometrically non-linear bar elements. The expression for the internal force vector and tangent stiffness matrix is developed from the principle of virtual work (PTV).

In implicit problems with a large number of elements (and degrees of freedom), the computational cost is dominated by solving the equations system. Therefore, as the beam model developed has half the degrees of freedom than the Euler-Bernoulli and Timoshenko beam elements (which have three translational and three rotational degrees of freedom per node), the implemented code has potential to result in greater computational efficiency. In explicit problems, no system of equations has to be solved and there is greater advantage.

The presented work details the derivation of the consistent tangent stiffness matrix for the elastic model, which is obtained by the exact calculation of the internal force derivative. As a consequence, quadratic convergence is achieved in the Newton-Raphson method. The analytical tangent stiffness matrix is also compared to the tangent matrix obtained by central finite differences, proving equality between them.

The simplified beam element is initially tested considering small displacements. For the simulation of a bi-supported beam, using forty elements, the error relative to elastic line is in the order of 0.5%, and for the clamped beam the errors do not exceed 1.0%.

Adopting large displacements, excellent agreement of results is also observed. The errors relative to software Msc Marc, for the bi-supported beam with forty elements are lower than 0.3%. For the clamped beam, excluding the boundary condition region, the errors are in the order of 0.25%. The transient behavior is also evaluated, obtaining a behavior very similar to that obtained by Msc Marc.

A linear generalized Maxwell viscoelastic model is developed for bending stiffness contribution in the simplified beam element. Transient results match very closely those provided by the software Msc Marc.

This implementation allows the analysis of various types of polymers, however, modeling HDPE demands continuity of the research to include non-linear viscoelasticity.

REFERENCES

[1] Karlsen, T. A. (2002), "Technical Catalogue for Submarine Installations of Polyethylene Pipes", PipeLifeNorge AS.

[2] Liu, H. (2007), "Material modelling for structural analysis of Polyethylene", Tese de doutorado, University of Waterloo.

[3] Palacios, J. G. (2004), "Análisis tensional del proceso constructivo de emisarios flotados y fondeados", Tese de doutorado, Universidad Politécnica de Madrid.

[4] Ghadimi, R. (1988), "A simple and Efficient Algorithm for the Static and Dynamic Analysis of Flexible Marine Risers", Vol. 29, Computers and Structures.

[5] Low, Y. M. and Langley, R. S. (2006), "Time and frequency domain coupled analysis of deepwater floating production systems", Vol. 28, Applied Ocean Research.

[6] Muñoz Rojas, P., Kühl, A., Mendonça, P. T. R., Benvenutti, I. and Creus, G. (2011), "Modeling Nonlinear Viscoelastic Behavior of High Density Polyethylene (HDPE): Application of Stress-Time Equivalence Versus Interpolation of Rheological Properties", MECSOL.

[7] Kaliske, H. and Rothert, H. (1997), "Formulation and implementation of three-dimensional viscoelasticity at small and finite strains", Springer Verlag.

[8] Park, S. W. and Schapery, R. A. (1999), "Methods of interconversion between linear viscoelastic material functions. Part I - a numerical method based on Prony series", Vol. 36, International Journal of Solids and Structures.

[9] Silva, H. N. (2009), "Caracterização Viscoelástica Linear de Misturas Asfálticas: Operacionalização Computacional e Análise pelo Método dos Elementos Finitos, Dissertação de mestrado", Universidade federal do Ceará.

[10] Brinson, H. F. and Brinson, L. C. (2008), Polymer Engineering Science and Viscoelasticity, An Introduction, Springer.

[11] Crisfield, M. (1991), Non-linear Finite Element Analysis of Solids and Structures, Vol. 1, first edition, John Wiley and Sons.

[12] Stahlschmidt, J. (2013), "Análise de Sensibilidade em Problemas Não Lineares via Método Semi-Analítico utilizando Variável Complexa: Aplicações em Parâmetros Materiais e Geométricos", Dissertação de mestrado a publicar, Universidade do Estado de Santa Catarina.

[13] Zienkiewicz, O., Watson, M. and King, I. (1968), "A Numerical Method of Visco-Elastic Stress Analysis", University of Wales.

[14] Johnson, A. R. (1999), "Modeling Viscoelastic Materials Using Internal Variables", Vol. 31, The Shock and Vibration Digest.